frontiers | Frontiers in Earth Science

TYPE Original Research
PUBLISHED 07 June 2023
DOI 10.3389/feart.2023.1132794

OPEN ACCESS

EDITED BY
Teresa Scolamacchia,
A.S.S.E.T. -Regione Puglia, Italy

REVIEWED BY
Barbara I. Kleine,
University of Iceland, Iceland
Bruce Christenson,
GNS Science, New Zealand

*CORRESPONDENCE
Victoria Kürzinger,
vkuerzinger@marum.de

RECEIVED 27 December 2022
ACCEPTED 24 May 2023
PUBLISHED 07 June 2023

CITATION
Kürzinger V, Hansen CT, Strauss H, Wu S and Bach W (2023), Experimental evidence for the hydrothermal formation of native sulfur by synproportionation. *Front. Earth Sci.* 11:1132794. doi: 10.3389/feart.2023.1132794

Experimental evidence for the hydrothermal formation of native sulfur by synproportionation

Victoria Kürzinger[1,2]*, Christian T. Hansen[1,2], Harald Strauss[3], Shijun Wu[4] and Wolfgang Bach[1,2]

[1]MARUM Center for Marine Environmental Sciences, University of Bremen, Bremen, Germany, [2]Faculty of Geoscience, University of Bremen, Bremen, Germany, [3]Institut für Geologie und Paläontologie, WWU Münster, Münster, Germany, [4]State Key Laboratory of Fluid Power and Mechatronic Systems, Zhejiang University, Hangzhou, China

Elemental sulfur (S^0) is known to form in submarine acid-sulfate vents by disproportionation of magmatic SO_2. S^0 formed upon disproportionation shows $\delta^{34}S_S$ values considerably lower than the influxing magmatic SO_2, which results in $\delta^{34}S_S$ values typically <0‰. The peculiar occurrence of isotopically heavy sulfur in the Kemp Caldera hydrothermal system ($\delta^{34}S_S$ > 5‰) and Niua North ($\delta^{34}S_S$ = 3.1‰) led to the suggestion that disproportionation is not the only sulfur forming process in submarine hydrothermal systems. We conducted hydrothermal experiments to investigate if synproportionation of SO_2 and H_2S can explain the occurrence and isotopic composition of S^0 observed in some vent fields. Provided that SO_2 and H_2S are both abundant, this formation mechanism is thermodynamically conceivable, but it has not yet been demonstrated experimentally that this process actually takes place in submarine hydrothermal systems. We conducted the experiments in collapsible Ti-cells under pT-conditions (20–30 MPa, 220°C) that are relevant to S^0 formation in submarine hydrothermal systems. We used starting concentrations of 10 mM sulfite and 20 mM sulfide of known isotopic composition. Under acidic conditions ($pH_{25\,°C}$ = 1.2), S^0 was the most abundant reaction product, but small amounts of sulfate were also produced. A Rayleigh fractionation model was applied to determine the isotopic composition of SO_4^{2-}, SO_2, H_2S and S^0 expected to form by SO_2 disproportionation, H_2S oxidation, and SO_2–H_2S synproportionation. The sulfur isotopic signatures of the sulfur produced in the experiments can only be explained by synproportionation of sulfite and sulfide. These results provide strong evidence that synproportionation is likely responsible for exceptionally high $\delta^{34}S_S$ values observed in S^0 from some arc/back-arc hydrothermal environments, like the Kemp Caldera in the South Sandwich arc. Coeval degassing of H_2S and SO_2 is likely required to have this particular reaction dominate in the H–S–O reaction network and produce noticeable accumulations of isotopically heavy native sulfur at the seafloor.

KEYWORDS

elemental sulfur (S^0), positive $\delta^{34}S$ values, synproportionation, experimental geochemistry, geochemical reaction path modeling

1 Introduction

In general, hydrothermal systems in arc/back-arc settings are enriched in volatiles like H_2O, CO_2, SO_2 and H_2S as a result of magma degassing (Reeves et al., 2011; Seewald et al., 2015; Wallace et al., 2015; Seewald et al., 2019). Hydrogen sulfide is not necessarily a direct product of magma degassing, but can also form through reduction of seawater sulfate or sulfur leaching from the host volcanic rock (Shanks et al., 1981).

It is well established that SO_2 is a major gaseous species in many arc magmas (e.g., Giggenbach, 1987; Fischer et al., 1998). Upon cooling and mixing with aqueous solutions in magmatic-hydrothermal systems, SO_2 is expected to disproportionate to sulfuric acid as well as both H_2S and elemental sulfur (see Eqs. 1, 2; Gamo et al., 1997; Kusakabe et al., 2000; Gena et al., 2006; Butterfield et al., 2011; de Ronde et al., 2011; Seewald et al., 2019):

$$4\,SO_{2\,(aq)} + 4\,H_2O = H_2S_{\,(aq)} + 3\,H_2SO_{4\,(aq)} \quad (1)$$

$$3\,SO_{2\,(aq)} + 2\,H_2O = S^0 + 2\,H_2SO_{4\,(aq)} \quad (2)$$

The sulfuric acid dissociates and gives rise to low pH and high sulfate concentrations in vents that are affected by this process (common in acid-sulfate vents). The sulfate formed in these submarine magmatic-hydrothermal systems by disproportionation reactions (1) and (2) has elevated $\delta^{34}S$ values (between ca. 17 and 25‰; de Ronde et al., 2005; McDermott et al., 2015; Peters et al., 2021) relative to the influxing magmatic SO_2 (4–10‰; Hannington et al., 2005). Elemental sulfur (S^0) produced alongside sulfate can have very low $\delta^{34}S$ values typically <0‰ like at the DESMOS caldera ($\delta^{34}S_S$ = −9.3‰; Gena et al., 2006) or at the Cone sites of Brothers volcano ($\delta^{34}S_S$ = −8.0‰; de Ronde et al., 2011). Likewise, dissolved sulfide and sulfide minerals in arc-hosted hydrothermal vent fluids typically show negative $\delta^{34}S$ values ($\delta^{34}S$ = −9.9 to −0.4‰), indicating SO_2 disproportionation (cf. Herzig et al., 1998; de Ronde et al., 2005; Gena et al., 2006; de Ronde et al., 2011; McDermott et al., 2015).

Although sulfides and elemental sulfur often have $\delta^{34}S$ values <0‰, positive values for S^0 have also been recently documented. In Niua North, an acid-sulfate vent in the northernmost Tonga arc, native sulfur exhibits a $\delta^{34}S$ value of 3.1‰ (Peters et al., 2021). In the Kemp Caldera of the South Sandwich island arc in the Scotia Sea samples of S^0 from acid-sulfate vent fields show even higher $\delta^{34}S$ values ranging from 5.2 to 5.8‰ (Figure 1; Kürzinger et al., 2022).

Peters et al. (2021) explained the large range of sulfur isotopic composition of sulfate, sulfide and native sulfur by variable SO_2 flux,

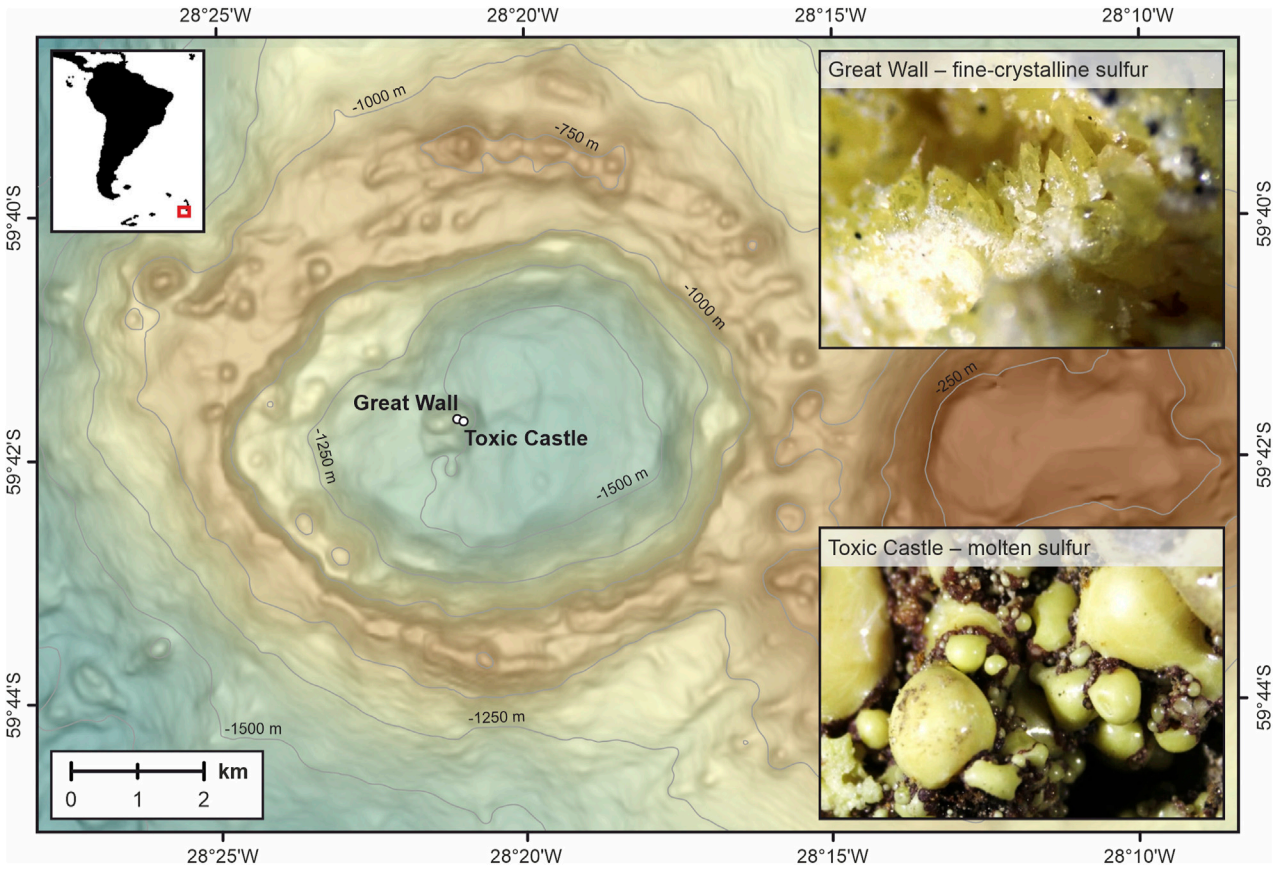

FIGURE 1
Bathymetric map of the submarine Kemp Caldera, which is located at the southernmost tip of the intra-oceanic South Sandwich arc. Elemental sulfur was sampled at the active white smoker vent fields Great Wall and Toxic Castle in the caldera center during the R/V *Polarstern* PS119 expedition in 2019.

disproportionation conditions, and host rock compositions. Their SO_2 disproportionation model for S^0, however, cannot fully explain the $\delta^{34}S$ value (3.1‰) of elemental sulfur at Niua North, unless the ingassing of an unusually ^{34}S-enriched SO_2 is assumed (Peters et al., 2021). The even higher $\delta^{34}S$ values from Kemp Caldera were found in the hydrothermally active area in the center at the eastern flank of a resurgent cone represented by the white smoker vent fields "Great Wall" and "Toxic Castle" (Figure 1). There, fluid venting at low to intermediate temperatures (60 to ~220°C) is associated with precipitation of elemental sulfur (Kürzinger et al., 2022). The molten S^0 from Toxic Castle shows $\delta^{34}S$ values between 5.2 and 5.5‰. An even higher value of 5.8‰ was measured at Great Wall from a fine-crystalline sulfur sample taken from the wall-like structure. These high $\delta^{34}S$ values suggest that disproportionation of magmatic SO_2 is unlikely the source of elemental sulfur at these sites. Oxidation of H_2S, proposed as a mechanism to explain ^{34}S-enriched elemental sulfur in terrestrial geothermal sites (Kleine et al., 2021) is implausible for submarine vent sites (Kürzinger et al., 2022).

Kürzinger et al. (2022) suggested synproportionation of SO_2 and H_2S to S^0 and water as an alternative to explain the observed high $\delta^{34}S$ values of the S^0:

$$SO_{2\,(aq)} + 2\,H_2S_{(aq)} = 3\,S^0 + 2\,H_2O \qquad (3)$$

It had been previously suggested that this synproportionation reaction is potentially a major sulfur forming mechanism of low-temperature fumaroles and solfataras in subaerial hydrothermal systems (Mizutani and Sugiura, 1966; Giggenbach, 1987; Chiodini et al., 1993). The elemental sulfur there is formed over a temperature range from <95 to >119°C (Mizutani and Sugiura, 1966). It was also hypothesized to play a role in the formation of liquid sulfur lakes in submarine volcanoes of intra-oceanic volcanic arcs, where the flux of magmatic volatiles is high (e.g., de Ronde et al., 2015). However, most accumulations of elemental sulfur at the seafloor have been explained by a high degassing flux of SO_2 followed by disproportionation to sulfur and sulfuric acid (Gamo et al., 1997; Butterfield et al., 2011; Seewald et al., 2015). This idea is corroborated by negative $\delta^{34}S$ values of sulfur that are expected to result from the disproportionation pathway of sulfur formation (e.g., Gamo et al., 1997; de Ronde et al., 2011; McDermott et al., 2015; Peters et al., 2021).

The first time SO_2–H_2S synproportionation was discussed in connection with sulfur formation in submarine arc volcano-hosted hydrothermal systems was in Kürzinger et al. (2022), who showed that SO_2–H_2S synproportionation may be exergonic not only in subaerial but also in submarine magmatic-hydrothermal systems that have high concentrations of SO_2 and H_2S. These authors also used a Rayleigh fractionation model to demonstrate that the isotopic composition of native sulfur from the Kemp Caldera, South Sandwich arc, is consistent with the synproportionation model. The synproportionation reaction of SO_2 and H_2S in aqueous solutions is expected to proceed much slower than in gas phase and it was unclear if the sulfur can form from within a single-phase aqueous solution or if sulfur condensed in a gas phase prior to dissolution of the gases in a hydrothermal solution.

To test the idea that elemental sulfur in submarine magmatic-hydrothermal systems may form by synproportionation in an aqueous solution, we conducted autoclave experiments in which we reacted dissolved SO_2 and H_2S under elevated pT-conditions. Sulfur concentrations and $\delta^{34}S$ values of reactants and reaction products were determined to discern plausible reaction pathways with respect to the fate of SO_2 (disproportionation *versus* synproportionation). The energetics of reaction (3) is examined and Rayleigh fractionation models for three S^0-forming reactions are presented. A reaction path model is introduced that explores which reactions contribute to the S^0-formation and how the isotopic compositions of reactants and reaction products evolve on the way to equilibrium.

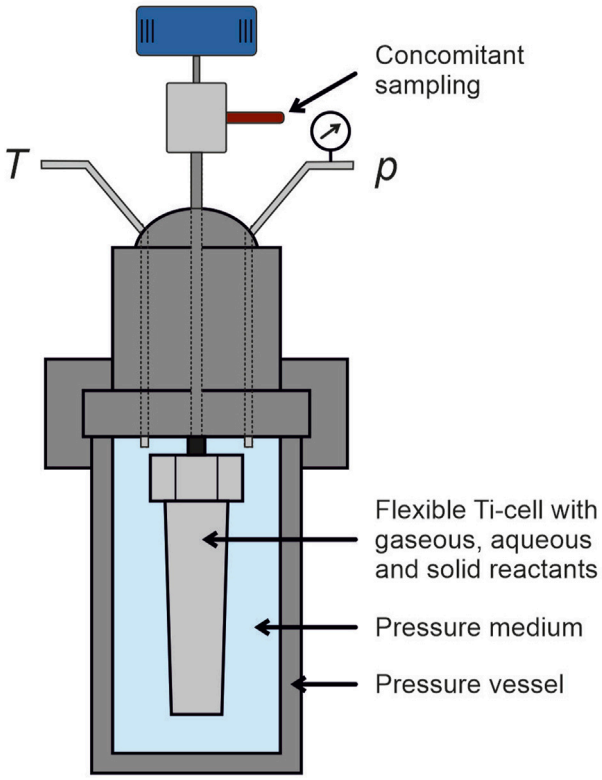

FIGURE 2
Scheme of the used hydrothermal reactor. The Dickson-type experimental setup consists of a pressure vessel that allows independent pressure and temperature control featuring a flexible titanium reaction cell from fluid samples that can be dawn over an access tube and valve made of titanium.

2 Methods

2.1 Experimental setup

Three experiments were conducted using a modified Dickson-type experimental setup that allows simulations of *in-situ* hydrothermal environment conditions (Dickson et al., 1963; Seyfried et al., 1987). Reactants (fluids and solids) reside within a collapsible container, which is sealed and mounted into a stainless-steal pressure vessel filled with distilled water (see Figure 2). Pressure of the water reservoir and the temperature of the vessel can be controlled independently (up to 400°C and 56.5 MPa). As the

TABLE 1 Specifications on the conducted experiments including initial amount of water (V_{water}) and hydrochloric acid ($V_{25\%\ HCl}$) as well as concentrations and sulfur isotopic characteristics of the initially introduced solid reactants ($Na_2S \cdot 3\ H_2O$, Na_2SO_3, S^0) and the ultimately retrieved (solid) product phases (S^0, SO_4 as $BaSO_4$, H_2S as Ag_2S, H_2). The pH-values were determined in the equilibrated final solution.

Components		Exp. #1	Exp. #2	Exp. #3
(1) Initial reactants				
V_{water}	[mL]	60.9	58.8	59.7
$V_{25\%\ HCl}$	[µL]	245	780	780
c_{sulfur}	[mmol/L]	1.59	1.23	0.46
$c_{sulfide}$	[mmol/L]	19.15	19.76	19.75
$c_{sulfite}$	[mmol/L]	9.64	9.93	9.89
n_{sulfur}	[µmol]	75	28	28
$n_{sulfide}$	[µmol]	1204	1204	1203
$n_{sulfite}$	[µmol]	605	603	603
$\delta^{34}S_{sulfur}$	[‰]	0.7	0.7	0.7
$\delta^{34}S_{sulfide}$	[‰]	6.7	6.7	6.7
$\delta^{34}S_{sulfite}$	[‰]	−2.8	−2.8	−2.8
(2) Final products				
Duration experimental run	[hrs]	24	24	24
$pH_{fluid\ (25\ °C)}$		7.8	1.2	1.1
c_{sulfur}	[mmol/L]	0.20	6.75	4.61
$c_{sulfide}$	[mmol/L]	0.26	0.24	0.11
$c_{sulfate}$	[mmol/L]	0.04	0.56	0.31
c_{H2}	[µmol/L]	n.d	n.d	5–10
n_{sulfur}	[µmol]	n.d	514	464
$n_{sulfide}$	[µmol]	n.d	94	41
$n_{sulfate}$	[µmol]	n.d	380	116
$\delta^{34}S_{sulfur}$	[‰]	−10.3	−0.3	0.4
$\delta^{34}S_{sulfide}$	[‰]	−4.1	0.8	1.5
$\delta^{34}S_{sulfate}$	[‰]	n.d	n.d	23.6

(--) means no measurement because material is not available, n.d.: not determined due to insufficient material. The underlined value marks the value of the recovered fine-crystalline sulfur formed during the experiment.

pressure is isostatically transferred to the contents of the collapsible cell, fluid sampling is enabled through a titanium access tube (featuring an in-line 0.2 µm mesh Ti-filter) and an attached custom fitted Ti-valve. Due to the reactivity of gold in H_2S-rich hydrothermal solutions we used a collapsible titanium foil cell (V_{tot} ~ 60 mL) instead of the more widely used cells made of gold (Hayashi and Ohmoto, 1991; Wu et al., 2016). Prior to the experiments, the Ti-cells were thoroughly cleaned with hydrochloric acid and heated to 400°C in air to create a surface layer of titanium oxide that is sufficiently inert under the targeted experimental conditions.

All three experiments were designed to investigate the isotopic fractionation of SO_2, H_2S and S^0, respectively, during the synproportionation reaction. The reactants sodium sulfide hydrate ($Na_2S \cdot 3\ H_2O$) and sodium sulfite (Na_2SO_3) were weighed and transferred into the titanium cell prefilled with ~60 mL of O_2-free ultrapure water (thoroughly purged with N_2). The reactants were weight into the cell to set a 20 mmol/L sulfide and 10 mmol/L sulfite concentration within approximately 60 mL of fluid (see Table 1; Supplementary Table S1). The concentrations for sulfide and sulfite were chosen in the milli-molal range to reflect typical concentrations of dissolved sulfur gases in submarine magmatic-hydrothermal systems (e.g., Butterfield et al., 2011; de Ronde et al., 2011; Seewald et al., 2015). The H_2S:SO_2 ratio of 2:1 is the same used by Mizutani and Sugiura (1966). A neglectable amount of elemental sulfur (between 0.9 and <2.5 mg) was added as seed crystals to prevent kinetic inhibition that can occur with homogenous nucleation.

Upon dissolution under hydrothermal conditions, these reactants provide the naturally occurring sulfide and sulfite for the experiments:

$$Na_2S \cdot 3\,H_2O + H_2O = HS^- + 2\,Na^+ + OH^- + 3\,H_2O \quad (4)$$

$$Na_2SO_3 + H_2O = HSO_3^- + 2\,Na^+ + OH^- \quad (5)$$

The OH^- released by reaction (4) and (5) causes the starting solution to be highly alkaline, which prevents degassing of sulfide and sulfite. However, the natural hydrothermal fluids are acidic and the neutral species H_2S and SO_2 dominate. The pH was therefore adjusted to a pH of 1.2 by adding <1 mL of 25% HCl (see Supplementary Table S1) right before the Ti-foil cell was sealed within the pressure vessel.

$$HS^- + OH^- + 2\,HCl = H_2S_{(aq)} + 2\,Cl^- + H_2O \quad (6)$$

$$HSO_3^- + OH^- + 2\,HCl = SO_{2\,(aq)} + 2\,Cl^- + 2\,H_2O \quad (7)$$

Thus, the starting fluid had 60 mmol/L of both Na^+ and Cl^- dissolved. The setup was then heated to approximately 220°C for approximately 24 h, while the pressure was maintained between 20 and 30 MPa.

2.2 Sampling and sample treatment

For the characterization of S^0, H_2S and SO_4^{2-}, 10 mL of sample were drawn from the reactor cell with a gastight syringe at experimental conditions after 24 h.

The samples were transferred into a vacuumed septum vial and 1 mL of 85% H_3PO_4 was added to enable a quantitative extraction of H_2S by means of N_2 purging (20 min) through a gas wash bottle prefilled with 20 mL of 5% $AgNO_3$ solution. Sulfide precipitated as Ag_2S flakes and was collected on a pre-weighed polycarbonate filter enabling a subsequent gravimetrical quantification. Next, 5 mL of the N_2-purged, acidified solution were transferred to a second vacuumed vial and 300 µL of a 1M $BaCl_2$ solution were added to precipitate any potentially present sulfate. In experiment #3, 600 µL of the 1M $BaCl_2$ solution were just added to the 10 mL sample in order to maximize the sulfate yield for subsequent isotopic characterization. Total amount of dissolved sulfate previously precipitated as $BaSO_4$ was subsequently derived by weight.

Concentrations and absolute contents for H_2S, SO_4^{2-} and S^0 given in Table 1 were derived by extrapolating the amounts retrieved from the respective sample volumes to the total fluid volume for each experiment.

An additional 1.75 mL of fluid were sampled into a gas tight syringe for the quantification of potentially formed H_2. Hydrogen was then quantified from about 0.25 mL gaseous headspace that unmixed from the fluid upon depressurization using an Agilent 7820 A gas chromatograph equipped with a 60/80 Molsieve column and a thermal conductivity detector.

2.3 Sulfur isotope measurements and computational methods

For sulfur isotope measurements, ca. 50 µg of elemental sulfur or 300–400 µg of silver sulfide are mixed with 400–800 µg of V_2O_5 and homogenized within a tin cup. Isotope measurements were carried out via elemental analyzer isotope ratio mass spectrometry (EA-IRMS) using a Flash EA IsoLink attached to a Thermo Fisher Scientific Delta V Advantage mass spectrometer. The reproducibility determined by replicate measurements was usually better than 0.3‰ (1σ). Analytical performance was controlled with IAEA-S1, -S2, -S3 and NBS 127 as international reference materials and with laboratory internal standards.

Using the initial isotopic composition of the reactants, we constructed a Rayleigh fractionation model (cf. McDermott et al., 2015; Kleine et al., 2021; Kürzinger et al., 2022). With this fractionation model we were able to predict sulfur isotopic compositions for all potential formation pathways and classify the measured values accordingly. Further details of the calculations are given in the Supplementary Material. Note: The isotopic composition of the reactants does not reflect the isotopic composition of naturally occurring sulfur species in magmatic-hydrothermal systems. Thus, the experimental isotope values will not mirror those measured in natural samples, but the magnitude and direction of isotope fractionation between the different sulfur species at given pT-conditions will be comparable.

Gibbs energies of reaction under experimental conditions were calculated for the sulfur formation reactions (syn- and disproportionation) as well as for the dissociation reactions of all involved sulfur species using the SUPCRT92 code (Johnson et al., 1992). The reaction path computation with Geochemist's Workbench (v. 12) makes use of a tailor-made database constructed for 25 MPa using SUPCRT92 and the OBIGT database (Dick, 2019). Equilibrium constants of all possible redox reactions (see Supplementary Figure S1) involving the four species H_2S, S^0, SO_2 and HSO_4^- are included in the database. These were derived essentially from prior experimental studies of sulfur hydrolysis and redox reactions (e.g., Ellis and Giggenbach, 1971).

The model is not a traditional titration path but instead it has the full amounts of SO_2 and H_2S in the system initially. All possible redox reactions are then kinetically inhibited to the same extent to investigate how the reaction network is predicted to evolve as the system approaches equilibrium state.

3 Results

3.1 Experimental results

Photographs of the experimental results as well as representative SEM images of elemental sulfur formed during the experiments are shown in Figures 3, 4.

For each experimental run, the individual steps were carried out as described above. During the first experiment (#1), precipitation of sulfur was not observed, although H_2S clearly had formed (strong characteristic smell) and the solution acquired a yellowish color. Sulfur precipitation only occurred following acidification with phosphoric acid for H_2S expulsion. Apparently, the synproportionation reaction does not proceed under alkaline conditions or kinetics are too sluggish for significant reaction turnover (previous pH ~ 7.8, see Table 1).

Accordingly, the follow-up experiments (#2 and #3) were run at conditions energetically more favorable for the synproportionation

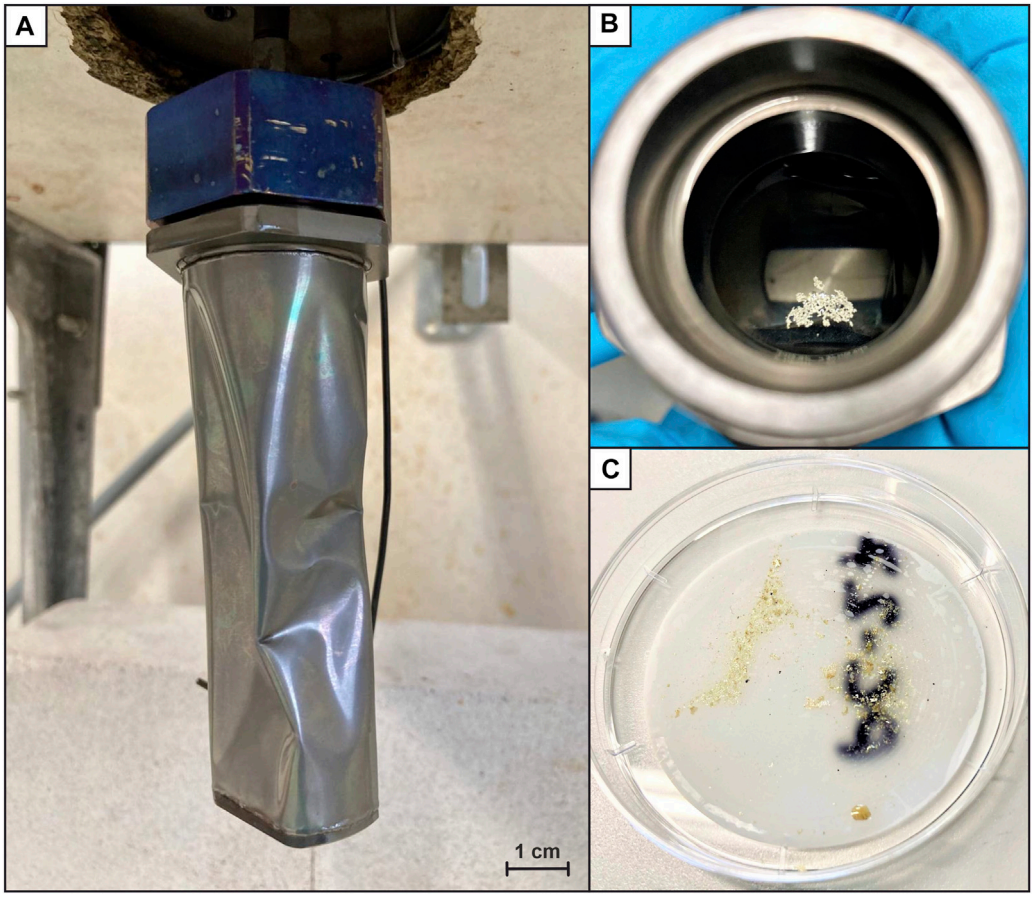

FIGURE 3
Images of the titanium reaction cell and the elemental sulfur formed during the last experiment. **(A)** Collapsed titanium cell after termination of the experiment, **(B)** View into the open cell: Elemental sulfur floating at the surface of the solution; additional sulfur quantities were found on the Ti-cell wall and bottom, and **(C)** Same fine-crystalline elemental sulfur as described in **(B)**, recovered on a polycarbonate filter.

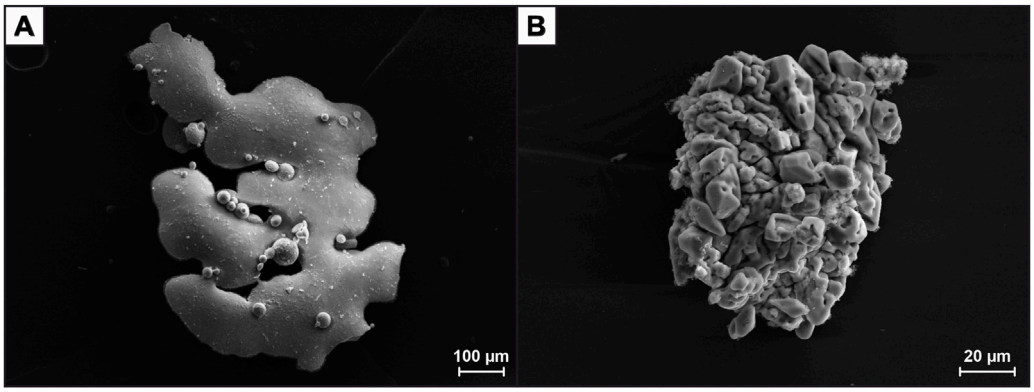

FIGURE 4
SEM images of elemental sulfur formed during experiment #2. **(A)** Sulfur particle from the subsample taken at 220°C. The appearance is similar to the molten sulfur at Toxic Castle (Kemp Caldera), and **(B)** Fine-crystalline sulfur recovered from the Ti reaction cell after finishing the experiment (cf. Figures 3B, C). These particles resemble sulfur from the Great Wall site in Kemp Caldera (cf. Figure 1).

reaction we suspect to take place at Toxic Castle in the Kemp Caldera hydrothermal system. The pH at Toxic Castle is likely lower than measured in 2019 ($pH_{25°C}$ = 5.7) due to seawater entrainment during sampling (see Kürzinger et al. (2022) for details). We hence adjusted the starting $pH_{25\ °C}$ to 2 in experiments #2 and #3, and native sulfur did form under these acidic conditions. Abundant fine-crystalline sulfur could then be recovered from the open titanium cell after terminating both experiments (Figure 3). Small sulfur flakes were visible even in the fluid sample extracted prior to the termination of the experiment, indicating that the sulfur did not form during cooling. Sulfate, only present in dissolved form, could be precipitated as $BaSO_4$ for a subsequent quantification (0.3–0.6 mmol/L). In addition, small amounts of H_2 could be quantified (5–10 µmol/L).

The sulfur recovered from experiments #2 and #3 had a very similar appearance compared to the sulfur samples from the Kemp Caldera (Figure 4). Some very fine-grained elemental sulfur (fitting through the 2 µm in-line Ti-filter) was removed from the cell into the syringe or precipitated from the solution upon rapid cooling and depressurization. This sulfur resembles the liquid S^0 at Toxic Castle (Figure 4A). On the other hand, the sulfur from the cooled reaction cell is fine-crystalline as it is at Great Wall (Figure 4B).

The amounts of sulfate (as $BaSO_4$) and sulfide (as Ag_2S) obtained from the subsamples (ca. 5 or 10 mL) and the elemental sulfur retrieved from the much larger residual volume left in the Ti-cell, i.e., ~45 or ~35 mL were both extrapolated to match the initial 60 mL (see Table 1). The total amounts of the different sulfur compounds retrieved from the experiment and their relative proportions indicate which reactions must have dominated in the system. Elemental sulfur is by far the most abundant, H_2S is only a small fraction of the initial amount, and sulfate concentration is also low. The experimental design is not geared towards full recovery of all species and phases, and hence the final concentrations reported do not add up to the amount of sulfur present in system (30 mmol/L in total or 1.8 mmol in the 60 mL volume of the reaction cell). We suspect that the missing sulfur is mainly represented by a coating on the inner walls of the reaction cell, which could not be fully retrieved after the experiment was terminated. A small fraction of the H_2S may be sorbed to elemental sulfur (e.g., Bacon et al., 1943).

3.2 Mass balance of sulfur species

Our experimental results indicate that the largest fractionation of the sulfur formed during the experiments could not have been due to SO_2 disproportionation. This can easily be seen by the data presented in Table 1. First, less than 0.1 mmol of the original 1.2 mmol sulfide in the reaction cell remained unreacted. This shows that sulfide was not produced during SO_2 disproportionation (Eq. 1), but instead it was consumed (such as in reaction 3). Second, disproportionation should produce twice as much sulfate than sulfur (see Eq. 2). But in the observed reaction product the amount of sulfur is greater than the amount of sulfate. The development of abundant elemental sulfur in concert with the pronounced drop in sulfide concentration can only be explained if synproportionation (Eq. 3) occurred in the reactor.

3.3 Sulfur isotopes

Isotopic compositions for the reactants $Na_2S \cdot 3\ H_2O$, Na_2SO_3 and S^0 (used as crystallization nucleus) were determined along with that of the S^0, H_2S and SO_4 fractions formed during the experiments (Table 1). Isotopic compositions for H_2S were determined from precipitated Ag_2S. Elemental sulfur in experiment #1 was only precipitated during sample processing and is clearly different in morphology from that produced in experiments #2 and #3. The sulfur produced in those later experiments has $\delta^{34}S$ values close to 0‰ in both instances (Table 1). The sulfur isotopic composition of H_2S is only 1.1‰ higher than those of S^0 which is consistent with an expected small equilibrium fractionation between native sulfur and H_2S (Ohmoto and Rye, 1979).

3.4 Sulfur isotope fractionation models

To further illuminate the sulfur formation process, we used the known initial isotopic composition of the reactants (Table 1) to construct a set of Rayleigh fractionation models for the different possible formation pathways (see Supplementary Material for details) and plotted the results together with the measured isotopic values of the sulfur recovered from the experiments (Figure 5). Another sulfur formation mechanism could be SO_4 reduction, but these values could not be calculated because we did not have an initial $\delta^{34}S_{SO4}$ value due to no existing sulfate at the beginning of the experiment.

The calculated values for H_2S oxidation as well as SO_2 disproportionation fall outside the measured range because they are either far too negative or too positive (see Figure 5). Thus, these reactions can be excluded as a possible sulfur formation process. However, the calculation results suggest that $\delta^{34}S_S$ values resulting from SO_2–H_2S synproportionation are consistent with the measured sulfur isotope values ($\delta^{34}S$ = −0.3 to 0.4‰) of elemental sulfur retrieved from experiments #2 and #3.

3.5 Thermodynamic/kinetic model

In addition to supposing specific sulfur redox reactions and studying their isotopic consequences, we conducted an arbitrary kinetics reaction path model computation to examine the predicted sequence in a hypothetical network of ten reactions (between the considered four oxidation states of sulfur (−2, 0, +4 and +6) there are 4!/((4–2)!*2!) = 6 possible simple redox reactions with two reaction partners and 4!/((4–3)!*3!) = 4 possible syn-/disproportionation reactions with three reaction partners; Supplementary Figure S1). The model predicts which of these reactions is expected to contribute how much to the total reaction turn-over as the system approaches equilibrium (Figure 6). Starting with initial concentrations of 10 mM SO_2 and 20 mM H_2S in the reaction cell (t = 0), two reactions are predicted to dominate in the first time-segment: (1) SO_2–H_2S synproportionation and (2) SO_2 disproportionation to S^0 and HSO_4^-. As SO_2 is consumed and HSO_4^- is produced in these reactions, the Gibbs energies of the reactions change. The affinity for the SO_2–H_2S synproportionation will go down, while those for reactions with HSO_4^- will go up. The

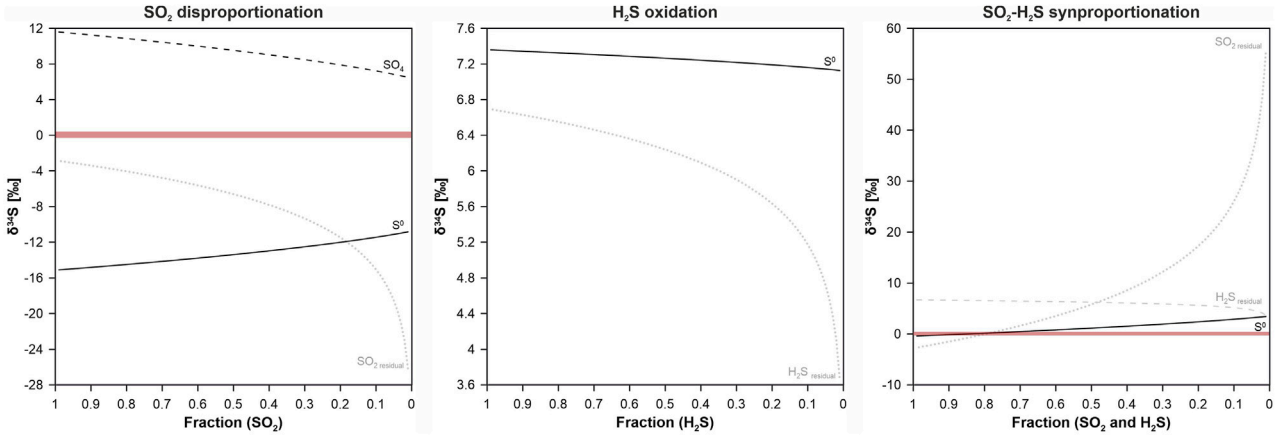

FIGURE 5
Results of expected $\delta^{34}S$ values for sulfur formed by SO_2 disproportionation, H_2S oxidation and synproportionation of SO_2 and H_2S at 220°C. The horizontal red bars represent the measured $\delta^{34}S$ values of elemental sulfur obtained from the experiments ($\delta^{34}S$ = −0.3 to 0.4‰). The calculated isotopic composition for H_2S oxidation ranging from 7.12 to 7.36‰ plot outside the measured $\delta^{34}S$ range of elemental sulfur. The $\delta^{34}S$ range for SO_2 disproportionation shows values between −15.1 and −10.6‰, which are far too negative. Only the sulfur values predicted for SO_2–H_2S synproportionation ($\delta^{34}S$ = −0.12 to 1.2‰) fit with the measured $\delta^{34}S$ values of sulfur.

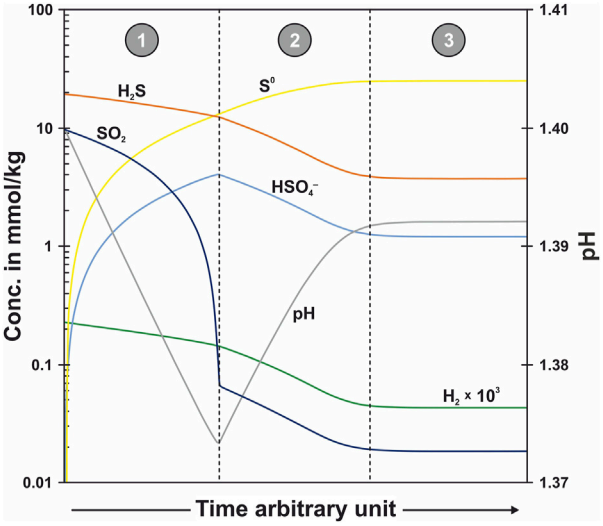

FIGURE 6
Results of an arbitrary kinetics reaction path model computation. The model has initial concentrations of SO_2 and H_2S that match those at the start of the experiment. The predicted sequence of reactions is dominated by SO_2–H_2S synproportionation and SO_2 disproportionation in time-segment 1 and by H_2S–HSO_4^- synproportionation (and subordinate SO_2–H_2S synproportionation) in time-segment 2, before equilibrium conditions are reached in time-segment 3.

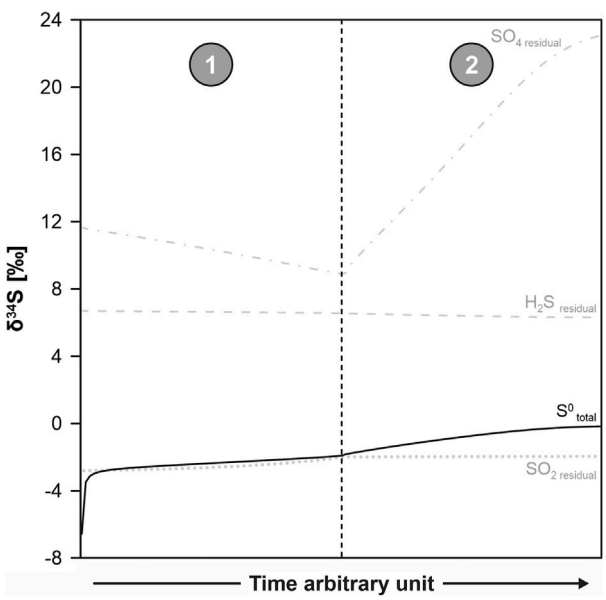

FIGURE 7
Rayleigh fractionation trends of the geochemical reaction path model presented in Figure 6. The predicted values for $\delta^{34}S$ of S^0 are close to 0‰, which is in accordance with the measured values. Correspondence can also be observed between predicted and measured isotopic compositions of sulfate. The model $\delta^{34}S$ of the residual H_2S is higher than what was measured.

transition from the first to the second time-segment is reached when the SO_2 disproportionation turns endergonic and H_2S–HSO_4^- synproportionation turns exergonic. SO_2–H_2S synproportionation continues to create small amounts of S^0. In reaching equilibrium, of the 30 mM total sulfur dissolved initially, 25 mM are predicted to have been converted to S^0, of which 23 mM are due to synproportionation (roughly equal contributions from SO_2–H_2S and H_2S–HSO_4^-) and 2 mM are due to SO_2 disproportionation. Equilibrium concentrations of H_2S and HSO_4^- are 3.7 and 1.2 mM, respectively.

In addition to instantaneous equilibrium isotope partitioning, we used the sulfur species abundances from the GWB reaction path model to compute Rayleigh fractionation trends. Kleine et al. (2021) suggested that Rayleigh fractionation more reliably represents isotope

TABLE 2 Log K, standard state Gibbs energy ($\Delta_R G^0$) and Gibbs energy ($\Delta_R G$) values for dis- and synproportionation reactions over a temperature range from 0 to 300°C and constant pressures (p = 30 MPa).

Temp. [°C]	Disproportionation[1]								Synproportionation[2]		
	$pH_{in\text{-}situ}$	Log K_1	γ_{HSO4}	γ_{SO4}	Log K	$\Delta_R G^0$	Log Q	$\Delta_R G$	Log K	$\Delta_R G^0$	$\Delta_R G$
0	1.20	−1.59	0.69	0.20	27.40	−143.29	4.68	−118.82	23.32	−121.94	−93.73
20	1.20	−1.81	0.69	0.20	24.46	−137.28	4.67	−111.05	21.20	−118.95	−88.67
40	1.22	−2.07	0.68	0.19	21.73	−130.29	4.71	−102.08	19.25	−115.38	−83.03
60	1.25	−2.34	0.67	0.18	19.21	−122.51	4.75	−92.19	17.47	−111.39	−76.98
80	1.28	−2.62	0.66	0.16	16.87	−114.04	4.80	−81.60	15.84	−107.08	−70.60
100	1.29	−2.91	0.65	0.15	14.69	−104.94	4.81	−70.62	14.35	−102.50	−63.94
120	1.30	−3.19	0.64	0.14	12.66	−95.26	4.81	−59.08	12.98	−97.71	−57.09
140	1.32	−3.48	0.62	0.13	10.75	−85.06	4.83	−46.88	11.75	−92.91	−50.23
160	1.34	−3.77	0.61	0.12	8.96	−74.30	4.85	−34.08	10.60	−87.93	−43.17
180	1.35	−4.06	0.59	0.11	7.26	−62.95	4.85	−20.90	9.54	−82.76	−35.94
200	1.38	−4.35	0.57	0.10	5.63	−51.01	4.88	−6.81	8.55	−77.42	−28.53
220	1.40	−4.65	0.56	0.09	4.07	−38.44	4.89	7.76	7.62	−71.91	−20.95
240	1.44	−4.95	0.53	0.07	2.56	−25.19	4.94	23.31	6.74	−66.22	−13.19
260	1.50	−5.26	0.51	0.06	1.10	−11.18	5.01	39.99	5.91	−60.34	−5.25
280	1.56	−5.59	0.48	0.05	−0.35	3.72	5.09	57.62	5.13	−54.27	2.88
300	1.67	−5.94	0.45	0.04	−1.80	19.69	5.25	77.34	4.37	−47.97	11.25

[1] $3\ SO_{2\ (aq)} + 2\ H_2O = S^0 + 2\ HSO_4^- + 2\ H^+$

[2] $SO_{2\ (aq)} + 2\ H_2S_{\ (aq)} = 3\ S^0 + 2\ H_2O$

$\Delta_R G = \Delta_R G^0 + 2.303\ R\ T\ Log\ Q$. In-situ pH and γ-values for HSO_4^- and SO_4^{2-} were calculated for a 400 mM NaCl solution with 20 mM SO_4^{2-}. The b-dot extended Debye-Hückel equation was used to calculate the activity coefficients following Helgeson (1969). The activities required to compute Log Q were calculated using the following concentrations: 10 mM for $SO_{2\ (aq)}$ and 20 mM for H_2S. The γ-values were assumed unity for neutral species. For the activity of HSO_4^-, fractions of HSO_4^- and SO_4^{2-} were calculated based on a total sulfate concentration of 20 mM and from the listed γ-values (for the dissociation reaction $HSO_4^- = SO_4^{2-} + H^+$).

fractionation in irreversible geochemical reactions in closed systems than the equilibrium partitioning supported by GWB. The evolution of isotopic composition of H_2S, S^0, SO_2, and HSO_4^- is shown in Figure 7. The correspondence between the measured and predicted isotopic compositions is excellent for S^0 and HSO_4^-. The measured $\delta^{34}S$ value of the leftover H_2S is lower than the predicted one.

4 Discussion

4.1 Experimental evidence for sulfur formation from synproportionation

The stability of elemental sulfur in water-bearing systems is known from experimental studies of sulfur hydrolysis to H_2S and SO_2 as well as H_2S and HSO_4^- (e.g., Ellis and Giggenbach, 1971). These reactions are the reverse of synproportionation discussed in this work. Formation of native sulfur by SO_2–H_2S synproportionation was already considered by Mizutani and Sugiura (1966) and Giggenbach (1987) as potential sulfur forming reactions in gaseous subaerial fumarole systems. Subequal amounts of both compounds in a cooling system will create thermodynamic drive for the reaction to proceed. Some H_2S is expected to form when SO_2 reacts with FeO in the rock through which the fumarole gas flows and undergoes cooling (Giggenbach, 1987). Hence low-temperature fumaroles in many volcanoes have both gases present in subequal amounts, and hence elemental sulfur can form by synproportionation of SO_2 and H_2S in the gas phase. It was unclear what the energetics and kinetics of the reaction in aqueous solutions under hydrothermal conditions are.

The energetics of native sulfur formation in an aqueous environment by synproportionation was examined by Kürzinger et al. (2022) for the Kemp Caldera, but the thermodynamic computations presented in this earlier communication were subject to large uncertainties in pH and sulfite concentrations of the hydrothermal fluids. Based on the new tight experimental constraints, we here reevaluate the energetics of the syn- and disproportionation pathways of elemental sulfur formation. For the measured low $pH_{25°C}$ of ~1.2 in experiments #2 and #3, the dissociation equilibrium is predicted to lie entirely on the undissociated side with sulfite and sulfide being dominated entirely by SO_2 and H_2S, respectively (see Figure 14 in Kürzinger et al., 2022). Results for $\Delta_R G$ for the dis- and synproportionation reactions over a temperature range from 0 to 300°C are listed in Table 2. They were calculated using the concentrations and activity coefficients (γ) provided in the footnote of Table 2 and are shown in Figure 8.

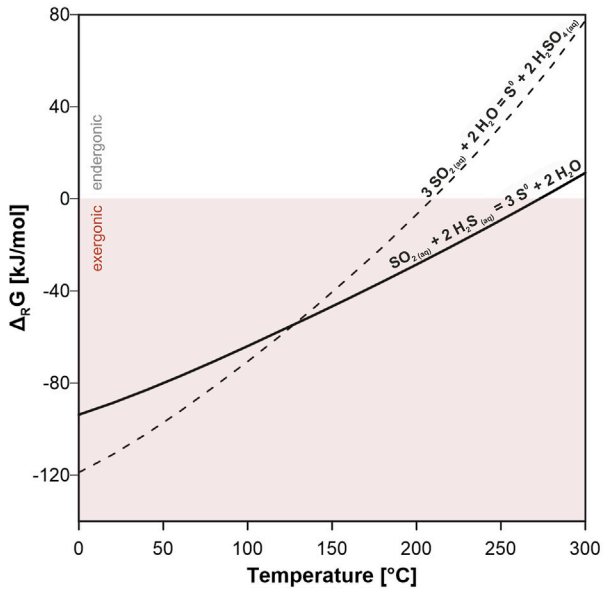

FIGURE 8
Gibbs energies per moles of disproportionation (3 $SO_{2\,(aq)}$ + 2 H_2O = S^0 + 2 $H_2SO_{4\,(aq)}$) and synproportionation ($SO_{2\,(aq)}$ + 2 $H_2S_{(aq)}$ = 3 S^0 + 2 H_2O) reactions as function of temperature at isobaric conditions (p = 30 MPa). Synproportionation stays exergonic up to 275°C, while disproportionation reaches a chemical equilibrium at ~210°C. See Table 2 for details.

At lower temperatures, both reactions are clearly exergonic, while the disproportionation reaction becomes endergonic at temperatures >210°C. Synproportionation, however, remains exergonic up to a temperature of about 275°C at the selected conditions (p = 30 MPa). From an energetic perspective, both reactions are likely to occur in the experiment. But even if the disproportionation reaction is endergonic at the target temperature of 220°C, this sulfur formation process cannot be entirely excluded. The experimentally produced elemental sulfur could have formed by disproportionation during the cooling phase as the system passed through the temperature range in which this reaction would be predicted to take place.

The elevated sulfate concentrations measured indicate that sulfate was formed by disproportionation reactions that took place subordinated to synproportionation. The reaction path model predicts that sulfate is formed by disproportionation alongside native sulfur early on in the reaction sequence. The predicted quantities are 2 mM of S^0 and 4 mM of sulfate. As SO_2 gets depleted and sulfate is enriched in solution, the energetics changes such that the synproportionation of sulfate and H_2S becomes exergonic, while sulfite-sulfide synproportionation continues with a small reaction turnover.

The formation of H_2 in the experiment, although in very small amounts of 5–10 µmol/L, indicates that another, subordinate reaction must have taken place in addition to the dominant synproportionation. A possible origin of the detected H_2 can be the partial oxidation of SO_2 with water as oxidant (Eq. 8).

$$SO_{2\,(aq)} + 2\,H_2O = HSO_4^- + H^+ + H_{2\,(aq)} \quad (8)$$

Using the concentrations and activity coefficients from Table 1 and 2 in concert with a calculated equilibrium constant (Log $K_{220\,°C}$ = 7.3) for Eq. 8, the measured H_2 concentrations correspond with the amount of H_2 predicted for equilibrium state in a pH 1.4 solution with 10 mM SO_2 and 2–6 mmol sulfate at 220°C. The reaction path model results suggest equilibrium concentrations of H_2 (4 µM) that are very close to the measured concentrations (Table 1). These results hence indicate that sulfate and SO_2 did indeed equilibrate in the hydrothermal apparatus. The formation of sulfuric acid plus H_2 by partial SO_2 oxidation could also explain why low pH may develop in systems in which SO_2 disproportionation is subordinate to SO_2–H_2S synproportionation.

In the conducted experiments, native sulfur was the most abundant sulfur species (4.6–6.75 mmol/L) and >10 times more abundant than sulfate (0.31–0.56 mmol/L) and sulfide (0.11–0.24 mmol/L). While the mass balance indicates that sulfur formation by synproportionation was dominant, the experimental setup was not optimized for allowing full retrieval of all sulfur species. It is hence not unexpected that the sum of the retrieved sulfur species does not add up to 30 mmol/L (the total sulfur concentration in the system). In the model, of the 25 mM S^0 produced, 2 mM are from SO_2 disproportionation and roughly 11.5 mM each are due to synproportionation of SO_2–H_2S and H_2S–HSO_4^-, respectively.

The predicted isotopic composition of the native sulfur (0‰) is also in agreement with the measured $\delta^{34}S$ values (cf. Table 1; Figure 5). The predicted $\delta^{34}S$ value of sulfate is in the range of 23‰ at 220 °C and very close to the measured value of 23.6‰. We hence suggest that the sulfate produced in the experiments has been formed by disproportionation and (to a lesser extent) by partial oxidation of the residual SO_2 (Eq. 8). As SO_2 is highly soluble in water and because of its intermediate oxidation state, it can act as reducing and oxidizing agent.

The residual H_2S has measured $\delta^{34}S$ values that are 1.1‰ higher than that of the S^0. The Rayleigh model predicts a higher $\delta^{34}S$ value (6.3‰) for H_2S than the 0.8‰–1.5‰ measured. Experimental data for H_2S–S^0 fractionation (Ohmoto and Rye, 1979) suggest that, in equilibrium, H_2S is 0.7‰ lighter than S^0. The measured difference of 1.1‰ is closer to the expected equilibrium value than the difference of the difference of 6.3‰ predicted by the Rayleigh model. This result may indicate that the small amount of H_2S left over in the experiment was close to equilibrium with the abundant S^0 that had formed primarily by synproportionation.

4.2 Implications for the isotopic composition of elemental sulfur in submarine arc/back-arc hydrothermal systems

Disproportionation of magmatic SO_2 in arc/back-arc magmatic-hydrothermal systems forms acid-sulfate type fluids with pH-values <3 (Gamo et al., 1997; Kim et al., 2009; de Ronde et al., 2011; Seewald et al., 2019). SO_2 degassing is common in these environments due to the oxidized nature of magma produced above a subducting slab (Wallace, 2005). Experimental and empirical studies (cf. Kusakabe et al., 2000; McDermott et al., 2015; Peters et al., 2021) have shown that the disproportionation-derived sulfate is enriched in ^{34}S, whereas the reduced counterparts (S^0 and H_2S) are depleted in ^{34}S relative to the isotopic composition of the influxing SO_2, which ranges between 4 and 10‰ in $\delta^{34}S$ (Hannington et al., 2005). The temperature-dependent

equilibrium isotope fractionation between aqueous SO_2, SO_4, S^0 and H_2S has been established (Ohmoto and Rye, 1979; Ohmoto and Lasaga, 1982; Kusakabe et al., 2000) and these constraints were used to compute the isotopic evolution of SO_2 and the products of the disproportionation reactions in hydrothermal fluids (McDermott et al., 2015; Kleine et al., 2021; Peters et al., 2021). The results from these studies suggest that the $\delta^{34}S$ values of elemental sulfur are typically <0‰ and those of the associated sulfate are commonly <21‰. The equilibrium isotope fractionation between native sulfur and H_2S is very small (Ohmoto and Rye, 1979), hence sulfides in arc/back-arc vent settings are usually also characterized by $\delta^{34}S$ values <0‰. Often, the $\delta^{34}S$ value of S^0 is lower than that of the dissolved H_2S (e.g., Peters et al., 2021), which may indicate that the S^0 formed at lower temperatures than the H_2S.

Although both sulfur and sulfide typically have negative values of $\delta^{34}S$, positive values for S^0 and H_2S have also been documented in various hydrothermal systems. For instance, hydrothermal fluids at Niuatahi volcano (NE Lau Basin) display positive $\delta^{34}S_{H2S}$ values ranging from 0.2 to 4.5‰ (Peters et al., 2021). Other examples include the Macauley and Brothers hydrothermal system, both hosted in submarine caldera volcanoes the Kermadec arc. The Macauley white smoker vent field is close to the summit of a dacitic cone near the SE caldera wall. Here, S^0 with a $\delta^{34}S$ value of −3.4‰ precipitates from highly acidic fluids with $\delta^{34}S_{H2S}$ values between 1.6 and 2.9‰ (Kleint et al., 2019; Peters et al., 2021). Brothers volcano hosts several chemically distinct active hydrothermal sites (e.g., de Ronde et al., 2005; de Ronde et al., 2011). Whereas the NW Caldera and Upper Caldera sites are dominated by black smoker-type fluids and Cu-Fe-rich sulfide chimneys, the Upper and Lower Cone vent fields are characterized by white smoker venting and the occurrence of elemental sulfur. Fluids of Brothers Upper Caldera show $\delta^{34}S$ values between 3.0 and 4.6‰ for dissolved sulfide (Kleint et al., 2019; Peters et al., 2021), while the Cone vent fluids are negative ($\delta^{34}S_{H2S}$ = −8.0 to −4.8‰; de Ronde et al., 2011). Niua, a volcano located in the northernmost Tonga arc, hosts two active vent sites ($\delta^{34}S_{H2S}$ = 2.6 to 4.5‰; Peters et al., 2021), but positive S^0 was only found at Niua North, exhibiting a $\delta^{34}S$ value of 3.1‰ (Peters et al., 2021). Even higher isotope values for elemental sulfur in the range from 5 to 6‰ from active vents in the Kemp Caldera (South Sandwich arc) were reported by Kürzinger et al. (2022). The very large range in the isotopic composition of sulfur and sulfide in arc/back-arc hydrothermal systems could be an indication of multiple pathways of sulfur formation mechanisms due to essential differences in redox, which allows for variable proportions of SO_2 and H_2S to be added to the hydrothermal system (cf. Kusakabe et al., 2000).

Kürzinger et al. (2022) proposed that the high $\delta^{34}S_S$ values observed in the Kemp Caldera are inconsistent with disproportionation of SO_2 and instead suggested that the S^0 is formed by SO_2–H_2S synproportionation. The experimental findings presented here provide irrefutable evidences that this novel S^0 formation pathway does indeed take place if energetically favorable conditions prevail. Our experimental results clearly show that the synproportionation of SO_2 and H_2S is a feasible process given that SO_2 and H_2S are both abundantly present. An essential requirement for the reaction to take place in nature is the simultaneous degassing of both SO_2 and H_2S. Work on fumarolic gases at convergent margin volcanoes (Giggenbach, 1987; Symonds et al., 1994; Moretti et al., 2013) has shown that the ratios of SO_2 and H_2S can be highly variable and that both gases can be abundant, in particular in low-temperature fumaroles.

If H_2S does not degas coevally with SO_2, disproportionation would then dominate in the reaction network controlling the sulfur speciation and isotopic fractionation. The common occurrence of isotopically light sulfur in submarine arc/back-arc hydrothermal systems suggests that SO_2 is frequently the dominant sulfur species added to hydrothermal systems by magma degassing. The observations of isotopically heavy sulfur in places like Niua North and the Kemp Caldera, however, are inconsistent with SO_2 disproportionation as formation process. Our work shows that synproportionation can be invoked to explain seafloor hydrothermal S^0 with such positive $\delta^{34}S$ values.

5 Summary and conclusion

We have presented three lines of evidence (mass balance, energetics and isotopic composition) to demonstrate that synproportionation can explain the formation of S^0 in our experiments. The experimental results presented in this study demonstrated the feasibility of SO_2–H_2S and possibly also synproportionation as additional pathway of S^0 formation in submarine magmatic-hydrothermal systems hosted in arc/back-arc settings. This pathway had been suggested to operate in fumarolic gases but is novel for aqueous systems. We demonstrate that SO_2–H_2S synproportionation to elemental sulfur does take place rapidly in single-phase aqueous solutions based on mass balance constraints, thermodynamic computations, and isotopic fractionation modelling. Specifically, the amount of S^0 formed in the experiments greatly exceeds the amount of experimentally produced sulfate. Also, at the pT-conditions of the experiments (20–30 MPa, 220°C), synproportionation of SO_2 and H_2S is energetically favorable, while SO_2 disproportionation is not. Finally, the experimentally generated elemental sulfur in this study has an isotopic composition that is consistent with values predicted by a Rayleigh fractionation model for synproportionation. Taken together, these results provide strong evidence that the sulfur formation mechanism by SO_2–H_2S synproportionation can not only occur in a fumarolic gas phase but also proceed in aqueous solutions of hydrothermal environments. The experimental findings and reaction path model results indicate that H_2S–HSO_4^- may also take place in systems with low SO_2 contents. The reactions went to completion within a day, indicating that these reactions are not kinetically inhibited in aqueous solutions.

We conclude that synproportionation of dissolved H_2S and oxidized sulfur species may represent a previously overlooked source of isotopically heavy sulfur in submarine magmatic-hydrothermal systems.

Data availability statement

The original contributions presented in the study are included in the article/Supplementary Material, further inquiries can be directed to the corresponding author.

Author contributions

VK, CTH and WB planned the study; VK and CTH conducted the experiments with support by SW; HS provided the S isotopic data; VK created all figures and wrote the first draft, CTH and WB helped interpretating data and write the paper, all authors read the paper and provided input; VK computed energetics and isotope fractionation assisted by WB; WB conducted the reaction path modelling.

Funding

Funding was provided by the Deutsche Forschungsgemeinschaft (DFG, German Research Foundation) under Germany's Excellence Strategy, EXC-2077—390741603. Earlier funding for building the hydrothermal apparatus was provided by a MARUM incentive fund to WB.

Acknowledgments

We thank P. Witte for the support with SEM-EDX analysis.

Conflict of interest

The authors declare that the research was conducted in the absence of any commercial or financial relationships that could be construed as a potential conflict of interest.

Publisher's note

Supplementary material

The Supplementary Material for this article can be found online at: https://www.frontiersin.org/articles/10.3389/feart.2023.1132794/full#supplementary-material

References

Bacon, R. F., and Fanelli, R. (1943). The viscosity of sulfur. *J. Am. Chem. Soc.* 65 (4). doi:10.1021/ja01244a043

Butterfield, D. A., Nakamura, K. I., Takano, B., Lilley, M. D., Lupton, J. E., Resing, J. A., et al. (2011). High SO2 flux, sulfur accumulation, and gas fractionation at an erupting submarine volcano. *Geology* 39 (9), 803–806. doi:10.1130/G31901.1

Chiodini, G., Cioni, R., and Marini, L. (1993). Reactions governing the chemistry of crater fumaroles from Vulcano Island, Italy, and implications for volcanic surveillance. *Appl. Geochem.* 8 (4), 357–371. doi:10.1016/0883-2927(93)90004-z

de Ronde, C. E. J., Chadwick, W. W., Ditchburn, R. G., Embley, R. W., Tunnicliffe, V., Baker, E. T., et al. (2015). "Molten sulfur lakes of intraoceanic arc volcanoes," in *Dmitri Rouwet, Bruce Christenson, Franco Tassi und Jean Vandemeulebrouck (Hg.): Volcanic Lakes* (Berlin, Heidelberg: Springer Berlin Heidelberg Advances in Volcanology, 261–288. doi:10.1007/978-3-642-36833-2_11

de Ronde, C. E. J., Hannington, M. D., Stoffers, P., Wright, I. C., Ditchburn, R. G., Reyes, A. G., et al. (2005). Evolution of a submarine magmatic-hydrothermal system: Brothers volcano, southern Kermadec arc, New Zealand. *N. Z.* 100 (6), 1097–1133. doi:10.2113/gsecongeo.100.6.1097

de Ronde, C. E. J., Massoth, G. J., Butterfield, D. A., Christenson, B. W., Ishibashi, J., Ditchburn, R. G., et al. (2011). Submarine hydrothermal activity and gold-rich mineralization at Brothers volcano, Kermadec arc, New Zealand. *Min. Deposita* 46 (5-6), 541–584. doi:10.1007/s00126-011-0345-8

Dick, J. M. (2019). Chnosz: Thermodynamic calculations and diagrams for geochemistry. *Front. Earth Sci.* 7. doi:10.3389/feart.2019.00180

Dickson, F. W., Blount, C. W., and Tunell, G. (1963). Use of hydrothermal solution equipment to determine the solubility of anhydrite in water from 100 degrees C to 275 degrees C and from 1 bar to 1000 bars pressure. *Am. J. Sci.* 261 (1), 61–78. doi:10.2475/ajs.261.1.61

Ellis, A., and Giggenbach, W. (1971). Hydrogen sulphide ionization and sulphur hydrolysis in high temperature solution. *Geochimica Cosmochimica Acta* 35 (3), 247–260. doi:10.1016/0016-7037(71)90036-6

Fischer, T. P., Giggenbach, W. F., Sano, Y., and Williams, S. N. (1998). Fluxes and sources of volatiles discharged from Kudryavy, a subduction zone volcano, Kurile Islands. *Earth Planet. Sci. Lett.* 160 (1-2), 81–96. doi:10.1016/S0012-821X(98)00086-7

Gamo, T., Okamura, K., Charlou, J.-L., Urabe, T., Auzende, J.-M., Ishibashi, J., et al. (1997). Acidic and sulfate-rich hydrothermal fluids from the Manus back-arc basin, Papua New Guinea. *Geology* 25 (2), 139–142. doi:10.1130/0091-7613(1997)025<0139:AASRHF>2.3

Gena, K. R., Chiba, H., Mizuta, T., and Matsubaya, O. (2006). Hydrogen, oxygen and sulfur isotope studies of seafloor hydrothermal system at the Desmos caldera, manus back-arc basin, Papua New Guinea: An analogue of terrestrial acid hot crater-lake. *Resour. Geol.* 56 (2), 183–190. doi:10.1111/j.1751-3928.2006.tb00278.x

Giggenbach, W. F. (1987). Redox processes governing the chemistry of fumarolic gas discharges from White Island, New Zealand. *Appl. Geochem.* 2 (2), 143–161. doi:10.1016/0883-2927(87)90030-8

Hannington, M. D., Ronde, C. D. J. de, and Petersen, S. (2005). "Sea-floor tectonics and submarine hydrothermal systems," in *Economic geology 100th anniversary volume. Littelton*. Editors J. W. Hedenquist, J. F. H. Thompson, R. J. Goldfarb, and J. P. Richards (Hg (Colorado, USA: Society of Economic Geologists), 111–114.

Hayashi, K., and Ohmoto, H. (1991). Solubility of gold in NaCl-and H2S-bearing aqueous solutions at 250–350°C. *Geochimica Cosmochimica Acta* 55 (8), 2111–2126. doi:10.1016/0016-7037(91)90091-I

Helgeson, H. C. (1969). Thermodynamics of hydrothermal systems at elevated temperatures and pressures. *Am. J. Sci.* 267 (7), 729–804. doi:10.2475/ajs.267.7.729

Herzig, P. M., Hannington, M. D., and Arribas, A., Jr. (1998). Sulfur isotopic composition of hydrothermal precipitates from the Lau back-arc: Implications for magmatic contributions to seafloor hydrothermal systems. *Mineral. Deposita* 33 (3), 226–237. doi:10.1007/s001260050143

Johnson, J. W., Oelkers, E. H., and Helgeson, H. C. (1992). SUPCRT92: A software package for calculating the standard molal thermodynamic properties of minerals, gases, aqueous species, and reactions from 1 to 5000 bar and 0 to 1000°C. *Comput. Geosciences* 18 (7), 899–947. doi:10.1016/0098-3004(92)90029-Q

Kim, J., Son, S.-K., Son, J.-W., Kim, K.-H., Shim, W. J., Kim, C. H., et al. (2009). Venting sites along the fonualei and northeast Lau spreading centers and evidence of hydrothermal activity at an off-axis caldera in the northeastern Lau Basin. *Geochem. J.* 43 (1), 1–13. doi:10.2343/geochemj.0.0164

Kleine, B. I., Gunnarsson-Robin, J., Kamunya, K. M., Ono, S., and Stefánsson, A. (2021). Source controls on sulfur abundance and isotope fractionation in hydrothermal fluids in the Olkaria geothermal field, Kenya. *Chem. Geol.* 582, 120446. doi:10.1016/j.chemgeo.2021.120446

Kleint, C., Bach, W., Diehl, A., Fröhberg, N., Garbe-Schönberg, D., Hartmann, J. F., et al. (2019). Geochemical characterization of highly diverse hydrothermal fluids from volcanic vent systems of the Kermadec intraoceanic arc. *Chem. Geol.* 528, 119289. doi:10.1016/j.chemgeo.2019.119289

Kürzinger, V., Diehl, A., Pereira, S. I., Strauss, H., Bohrmann, G., and Bach, W. (2022). Sulfur formation associated with coexisting sulfide minerals in the Kemp Caldera hydrothermal system, Scotia Sea. *Chem. Geol.* 606, 1–20. doi:10.1016/j.chemgeo.2022.120927

Kusakabe, M., Komoda, Y., Takano, B., and Abiko, T. (2000). Sulfur isotopic effects in the disproportionation reaction of sulfur dioxide in hydrothermal fluids: Implications for the δ 34 S variations of dissolved bisulfate and elemental sulfur from active crater lakes. *Geology* 97 (1-4), 287–307. doi:10.1016/S0377-0273(99)00161-4

McDermott, J. M., Ono, S., Tivey, M. K., Seewald, J. S., Shanks, W. C., and Solow, A. R. (2015). Identification of sulfur sources and isotopic equilibria in submarine hot-springs using multiple sulfur isotopes. *Geochimica Cosmochimica Acta* 160, 169–187. doi:10.1016/j.gca.2015.02.016

Mizutani, Y., and Sugiura, T. (1966). The chemical equilibrium of the 2H 2 S+SO 2 =3S+2H 2 O reaction in solfataras of the nasudake volcano. *BCSJ* 39 (11), 2411–2414. doi:10.1246/bcsj.39.2411

Moretti, R., Arienzo, I., Civetta, L., Orsi, G., and Papale, P. (2013). Multiple magma degassing sources at an explosive volcano. *Earth Planet. Sci. Lett.* 367, 95–104. doi:10.1016/j.epsl.2013.02.013

Ohmoto, H., and Lasaga, A. C. (1982). Kinetics of reactions between aqueous sulfates and sulfides in hydrothermal systems. *Geochimica Cosmochimica Acta* 46 (10), 1727–1745. doi:10.1016/0016-7037(82)90113-2

Ohmoto, H., and Rye, R. O. (1979). "Isotopes of sulfur and carbon," in *Geochemistry of hydrothermal ore deposits. 2*. Editor L. Hg HubertBarnes (Edition: John Wiley and Sons, Inc.), 509–567.

Peters, C., Strauss, H., Haase, K., Bach, W., Ronde, C. E. de, Kleint, C., et al. (2021). SO2 disproportionation impacting hydrothermal sulfur cycling: Insights from multiple sulfur isotopes for hydrothermal fluids from the Tonga-Kermadec intraoceanic arc and the NE Lau Basin. *Chem. Geol.* 586, 120586. doi:10.1016/j.chemgeo.2021.120586

Reeves, E. P., Seewald, J. S., Saccocia, P., Bach, W., Craddock, P. R., Shanks, W. C., et al. (2011). Geochemistry of hydrothermal fluids from the PACMANUS, northeast pual and vienna woods hydrothermal fields, manus basin, Papua New Guinea. *Geochimica Cosmochimica Acta* 75 (4), 1088–1123. doi:10.1016/j.gca.2010.11.008

Seewald, J. S., Reeves, E. P., Bach, W., Saccocia, P. J., Craddock, P. R., Shanks, W. C., et al. (2015). Submarine venting of magmatic volatiles in the eastern manus basin, Papua New Guinea. *Geochimica Cosmochimica Acta* 163, 178–199. doi:10.1016/j.gca.2015.04.023

Seewald, J. S., Reeves, E. P., Bach, W., Saccocia, P. J., Craddock, P. R., Walsh, E., et al. (2019). Geochemistry of hot-springs at the SuSu Knolls hydrothermal field, Eastern Manus Basin: Advanced argillic alteration and vent fluid acidity. *Geochimica Cosmochimica Acta* 255, 25–48. doi:10.1016/j.gca.2019.03.034

Seyfried, W. E., Janecky, D. R., and Berndt, M. E. (1987). "Rocking autoclaves for hydrothermal experiments II. The flexible reaction-cell system," in *Hydrothermal experimental techniques* (New Jersey, USA: Wiley-Interscience Publications), 216–239.

Shanks, W., Bischoff, J. L., and Rosenbauer, R. J. (1981). Seawater sulfate reduction and sulfur isotope fractionation in basaltic systems: Interaction of seawater with fayalite and magnetite at 200–350°C. *Geochimica Cosmochimica Acta* 45 (11), 1977–1995. doi:10.1016/0016-7037(81)90054-5

Symonds, R. B., Rose, W. I., Bluth, G. J., and Gerlach, T. M. (1994). Volatiles in magmas. *Rev. Mineralogy* 30, 1–66.

Wallace, P. J., Plank, T., Edmonds, M., and Hauri, E. H. (2015). "Volatiles in magmas," in *Encyclopedia of volcanoes*. Editor B. F. Hg Haraldur Sigurdsson undHoughton. Second edition (Amsterdam, Boston: Elsevier/AP, Academic Press is an imprint of Elsevier), 163–183. doi:10.1016/B978-0-12-385938-9.00007-9

Wallace, P. J. (2005). Volatiles in subduction zone magmas: Concentrations and fluxes based on melt inclusion and volcanic gas data. *Geology* 140 (1-3), 217–240. doi:10.1016/j.jvolgeores.2004.07.023

Wu, S.-J., Cai, M.-J., Yang, C.-J., and Li, K.-W. (2016). A new flexible titanium foil cell for hydrothermal experiments and fluid sampling. *Rev. Sci. Instrum.* 87 (9), 095110–095116. doi:10.1063/1.4963700